

The utility of cardiac MRI in diagnosis of infective endocarditis: preliminary results

Memduh Dursun, Sabri Yılmaz, Erdem Yılmaz, Ravza Yılmaz, İmran Onur, Hüseyin Oflaz, Aygün Dindar

PURPOSE

We aimed to evaluate the utility of cardiac magnetic resonance imaging (MRI) for the diagnosis of infective endocarditis (IE).

METHODS

Sixteen patients with a preliminary diagnosis of IE (10 women and six men; age range, 4–66 years) were referred for cardiac MRI. MRI sequences were as follows: echo-planar cine true fast imaging with steady-state precession (true-FISP), dark-blood fast spin echo T1-weighted imaging, T2-weighted imaging, dark-blood half-Fourier single shot turbo spin echo (HASTE), and early contrast-enhanced first-pass fast low-angle shot (FLASH). Delayed contrast-enhanced images were obtained using three-dimensional inversion recovery FLASH after 15±5 min. The MRI features were evaluated, including valvular pathologies on cine MRI and contrast enhancement on the walls of the cardiac chambers, major thoracic vasculature, and paravalvular tissue, attributable to endothelial extension of inflammation on contrast-enhanced images.

RESULTS

Fourteen valvular vegetations were detected in eleven patients on cardiac MRI. It was not possible to depict valvular vegetations in five patients. Vegetations were detected on the aortic valve (n=7), mitral valve (n=3), tricuspid and pulmonary valves (n=1). Delayed contrast enhancement attributable to extension of inflammation was observed on the aortic wall and aortic root (n=11), paravalvular tissue (n=4), mitral valve (n=2), walls of the cardiac chambers (n=6), interventricular septum (n=3), and wall of the pulmonary artery and superior mesenteric artery (n=1).

CONCLUSION

Valvular vegetation features of IE can be detected by MRI. Moreover, in the absence of vegetations, detection of delayed enhancement representing endothelial inflammation of the cardiovascular structures can contribute to the diagnosis and treatment planning of IE.

The definition of infective endocarditis (IE) has now been expanded from infection of leaflets and chordae found in cardiac cavities, to infection of any structure in the heart, including the endothelial surface, valves, and myocardium, as well as prosthetic valves and implanted devices (1). Cardiac endothelium and valves are generally resistant to bacterial and fungal infection. However, some highly virulent microbial pathogens are capable of infecting normal cardiac valves (2). Animal studies suggest that the first stage of infection is endothelial damage, followed by deposition of platelet-fibrin, which sets the stage for bacterial colonization (3). Infection may also expand to the tissues surrounding the leaflets, including the sinotubular junction, annulus, myocardium, and the conduction system (1).

There have been developments in treatment of IE, as well as prevention and detection of possible complications. Nevertheless, hospital mortality remains at the high rate of 20% (4). Despite advances in diagnostic methods, diagnosis is complicated as IE does not exhibit specific clinical signs in the early stage and has variable features (5). The diagnostic criteria for IE, known as the Duke criteria, were defined by Durack et al., in 1994 (6). These criteria have recently been expanded to include the use of transthoracic echocardiography and microbial antibody titers, and the proposed changes have been published and confirmed by other authors (1).

While computed tomography (CT) and magnetic resonance imaging (MRI) are common modalities in diagnosis of stroke and embolic events, their functionality in cardiac pathology imaging is not entirely clear. Several studies report using MRI for diagnosis of IE (7–10), but no large series studies have been conducted to date.

Diagnosis of IE by cross-sectional imaging has been restricted to depiction of valvular vegetations and other valvular pathologies. However, diagnosis of IE based on contrast enhancement pattern of the endothelial lining on MRI has not been previously studied. In the present study, in addition to the depiction of valvular pathologies on cine MRI, contrast enhancement pattern of the endothelial lining was evaluated by early and delayed contrast-enhanced images to contribute to the diagnosis of IE.

Methods

Patient population

The study population consisted of 16 patients (10 women and six men; age range, 4–66 years) with a preliminary diagnosis of IE by clinical, laboratory, and echocardiographic findings. This study was approved by the hospital ethics committee. Informed consent was obtained from all patients. All patients had fever between 37.5°C and 39.5°C measured at the

From the Departments of Radiology (M.D., E.Y. ✉ yilmazerdem79@yahoo.com.tr, R.Y.), Cardiology (I.O., H.O.), and Pediatric Cardiology (A.D.), Istanbul University, Istanbul School of Medicine, Istanbul, Turkey; and the Department of Pediatric Radiology (S.Y.), University of Pittsburgh School of Medicine, Pittsburgh, USA.

Received 11 June 2014, revision requested 21 July 2014, revision received 1 August 2014, accepted 8 August 2014.

Published online 25 November 2014.
DOI 10.5152/dir.2014.14239

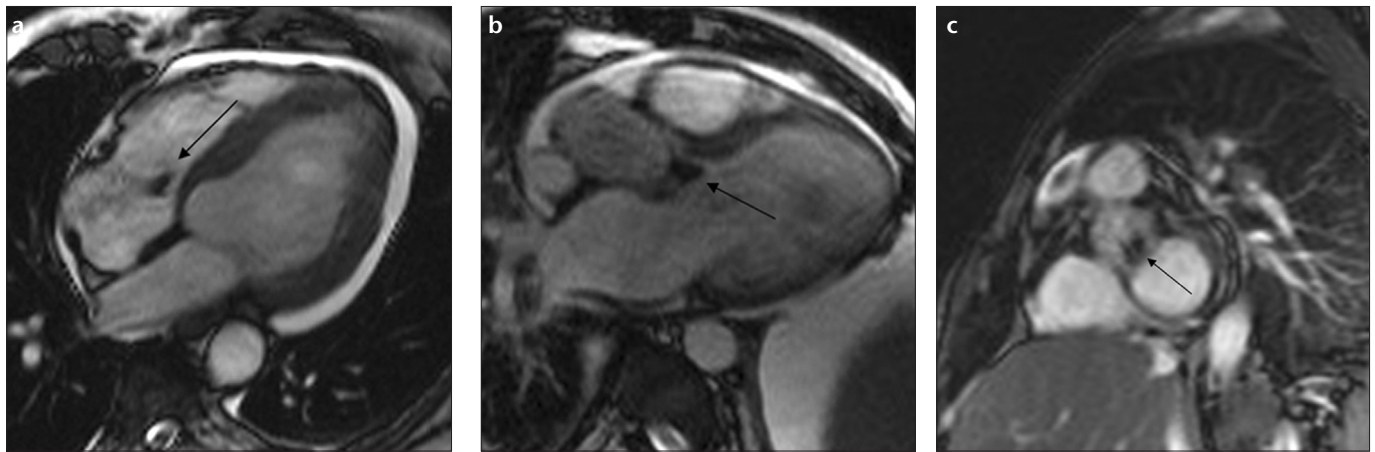


Figure 1. a–c. Vegetations observed in three different patients on cine MRI. Single vegetations (*arrows*) are noticed on the tricuspid valve (**a**) and the aortic valve (**b**). Panel (**c**) shows two vegetations detected on the aortic valve (*arrow*).

axilla. Other common symptoms were weakness, dyspnea, and cough. Cardiac examination revealed murmur in all patients, except one. On echocardiographic examinations eight patients had valvular pathology on the aortic valve, four on the mitral valve, two on the tricuspid valve and one on the pulmonary valve. One patient, a six-year-old girl, had a history of surgery for tetralogy of Fallot five years earlier, and no valvular pathology was seen in this patient. Laboratory tests showed high levels of erythrocyte sedimentation rate and high white blood cell count in all patients.

All 16 patients underwent transthoracic echocardiography (TTE) examination and 12 patients additionally underwent transesophageal echocardiography (TEE) examination. TEE could not be completed in six of 12 patients because they could not tolerate the examination. Repeated echocardiographic examinations were performed in seven patients either for diagnosis or for follow-up. No vegetation was observed in one patient with a strong suspicion of IE, although he underwent three sessions of TTE and two sessions of TEE. Two patients were examined twice with TTE and twice with TEE, whereas the remaining four patients were evaluated twice with TTE and once with TEE for follow up.

MRI indications were as follows: absence of vegetation in TTE or TEE exams in four patients, inability to tolerate TEE in six patients, and differential diagnosis of vegetation and intracardiac mass in six patients.

MRI

MRI was performed on a 1.5 T scanner (Symphony, Siemens Medical Systems, Erlangen, Germany) with electrocardiographic triggering. The MRI sequences and parameters were as follows: echo-planar cine true fast imaging with steady-state precession (FISP) imaging (TR/TE, 50/1.70 ms; matrix, 256×256; slice thickness, 6 mm); dark-blood fast spin echo T1-weighted (TR/TE, 700/26 ms; matrix, 133×256; slice thickness, 5 mm), T2-weighted (TR/TE, 1600/81 ms; matrix, 133×256; slice thickness, 5 mm), dark-blood half-Fourier single shot turbo spin echo (HASTE) (TR/TE, 800/26 ms; matrix, 256×256; slice thickness, 6 mm), early contrast-enhanced first-pass fast low-angle shot (FLASH) (TR/TE, 257/1.11 ms; matrix, 128×256; slice thickness, 6 mm) and delayed contrast-enhanced images were obtained using three-dimensional (3D) inversion recovery FLASH (TR/TE, 750/1.58 ms; time to inversion, 260 ms; matrix, 256×256; slice thickness, 4 mm) after 15±5 min. Images were evaluated for valvular pathologies including vegetation, stenosis, or insufficiency, and also, for early and delayed contrast enhancement of the walls of cardiac chambers and major arteries and of the paravalvular tissue.

Results

Overall, 14 vegetations were detected in 11 out of 16 patients on cardiac MRI (Fig. 1, Table). Vegetations were found on the aortic valve in seven patients, with one patient having two vegetations. The largest vegetation (15×16

mm) was found on the aortic valve of a 47-year-old man, who also had stenosis on the aortic valve. In this patient, delayed contrast enhancement secondary to dissemination of the infection was observed on the paravalvular tissue and on the aortic wall (Fig. 2). Another patient, a 48-year-old man, had an aortic valve vegetation sized 7×9.5 mm which was visible only on MRI, although signal changes concordant with aortic valve insufficiency were also present on repeated TTE and TEE examinations. Furthermore, delayed contrast enhancement was observed on the mitral valve, all segments of the aorta, and the wall of the superior mesenteric artery (Fig. 3). Two other patients aged 14 and 18 years, had aortic valve vegetations and delayed contrast enhancement on the aortic wall. Additionally, a 14-year-old patient had delayed contrast enhancement on the subendocardium of the interventricular septum. No delayed contrast enhancement was observed in the remaining two patients who had aortic valve vegetations. Tricuspid valve vegetation was seen in a 53-year-old man. Contrast enhancement was observed on the lateral wall of the right ventricle and the wall of aorta.

Another 14-year-old patient had pulmonary valve vegetation. Delayed contrast enhancement was detected on the paravalvular area, pulmonary artery wall, and lateral wall of the right ventricle.

MRI showed two vegetations on the mitral valve and contrast enhancement on the paravalvular area, in the interventricular septum, and on the wall of the aorta in an 11-year-old girl

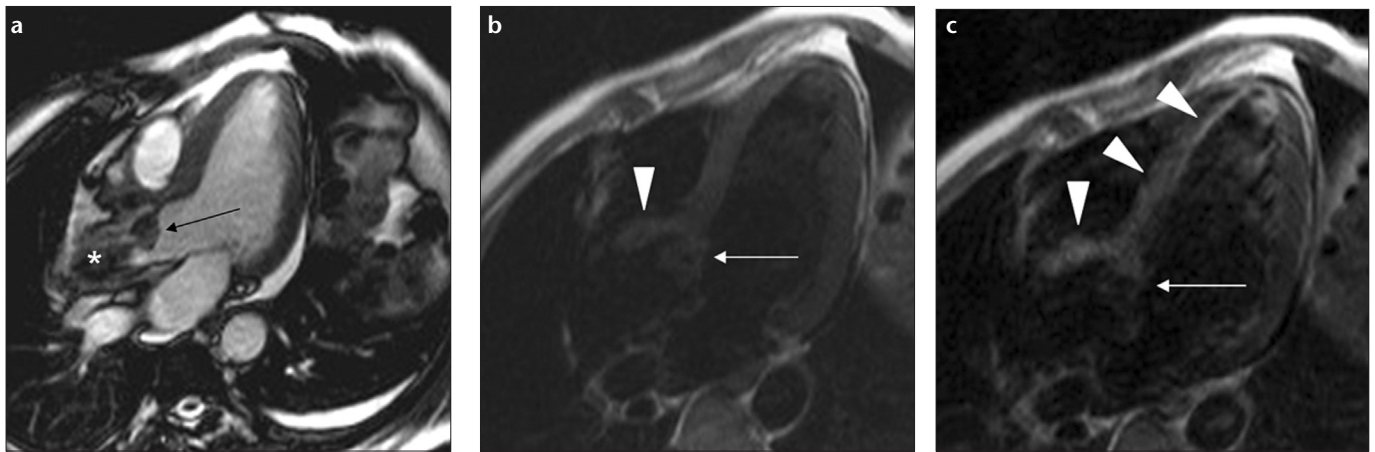


Figure 2. a–c. Direct extension of IE to the paravalvular tissue and interventricular septum in a 47-year-old male on cardiac cine MRI. Cine image (a) shows a large vegetation on the aortic valve (arrow) and signal changes of blood flow secondary to severe stenosis in the aorta (asterisk). Precontrast T1-weighted image (b) shows a hypointense vegetation (arrow), paravalvular tissue, and interventricular septum (arrowhead). Contrast enhancement of the vegetation (arrow), paravalvular tissue, and interventricular septum (arrowheads) is seen secondary to direct extension of IE (c).

Table. Distribution of valvular vegetations and delayed contrast enhancement secondary to dissemination of the infection on MRI

Patient age, sex	Affected valves	Vegetation size (mm)	Location of delayed contrast enhancement
42, F	Aortic	7×12, 8×11	-
47, M	Aortic	15×16	Aortic wall, paravalvular tissue
48, M	Aortic	7×9.5	Aortic and SMA wall, mitral valve
14, F	Aortic	9×10	Aortic wall, IVS
18, M	Aortic	11×12	Aortic wall
35, F	Aortic	8×13	-
53, M	Tricuspid	7×10	Aortic wall, RV lateral wall
14, F	Pulmonary	10×13	PA wall, RV lateral wall, paravalvular tissue
11, F	Mitral	9×11, 8×12	Aortic wall, IVS, paravalvular tissue
66, F	Mitral	6×12	Aortic wall, LA wall, mitral valve
33, M	Mitral and aortic	9×11, 7×10	-
60, F	-	-	Aortic root, LA wall, paravalvular area
4, F	-	-	Aortic root, RV lateral wall, IVS
58, F	-	-	Aortic wall, both atrium walls
55, M	-	-	-
6, F	-	-	Aortic wall

M, male; F, female; SMA, superior mesenteric artery; IVS, interventricular septum; RV, right ventricle; PA, pulmonary artery; LA, left atrium.

(Fig. 4). Additionally, significant trabeculation concordant with ventricular non-compaction in the left ventricle was observed in this patient. A mitral valve vegetation sized 6×12 mm was detected on MRI in a 66-year-old woman. Furthermore, delayed contrast enhancement was observed on the mitral valve, ascending aorta, and the wall of the left atrium. No delayed

contrast enhancement was observed in a 33-year-old man, who had two vegetations, one lesion on the aortic valve and one on the mitral valve.

The vegetations were not detectable by MRI in the remaining five patients, despite two vegetations being clearly visualized by TTE prior to MRI. In one patient, it was not possible to detect the vegetation because of an artifact

caused by the mitral valve prosthesis. Contrast enhancement was observed in the left atrium, mitral paravalvular area, and the aortic root in this patient. The second patient, a four-year-old girl, in whom vegetation was observed on echocardiography but not on MRI, had received long-term antibiotherapy before the MRI examination. In addition, contrast enhancement was observed on the aortic root, the lateral wall of the right ventricle, and on the right surface of the proximal interventricular septum, together with a small ventricular septal defect (VSD) (Fig. 5).

Vegetation was not observed by echocardiography or cardiac MRI in a 58-year-old woman. However, cardiac MRI showed delayed enhancement on the wall of both atriums and the aortic wall. No abnormalities were observed in a 55-year-old man, because the patient had received long-term antibiotherapy before the MRI.

Despite a high suspicion of IE, vegetation was seen neither by cardiac MRI nor with TTE in a six-year-old girl, who had surgery for tetralogy of Fallot five years earlier. Even though no vegetation was detected on cardiac valves, delayed contrast enhancement was seen on the wall of the descending aorta.

No early contrast enhancement was visualized in patients who showed delayed contrast enhancement.

Discussion

The incidence of IE is estimated at 1.9–6.2 per 100.000 patient-years, and

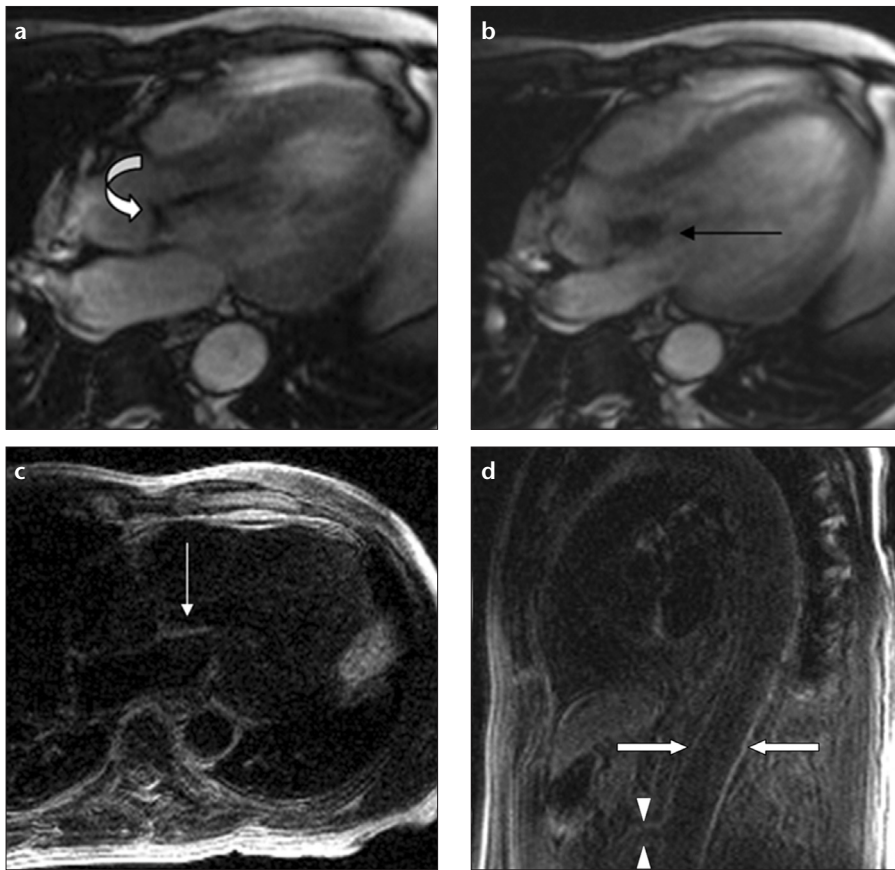


Figure 3. a–d. Antegrade and retrograde extension of IE in a 48-year-old male with aortic insufficiency. Panel (a) shows leaflet thickening secondary to vegetation on the aortic valve (*curved arrow*). Panel (b) shows a jet flow towards the anterior leaflet of the mitral valve due to aortic insufficiency (*arrow*). Delayed contrast-enhanced image (c) shows retrograde extension of the infection on the anterior leaflet of the mitral valve (*arrow*). Panel (d) shows delayed contrast enhancement on the endothelium of the aorta (*arrows*) and superior mesenteric artery wall (*arrowheads*) secondary to antegrade extension of IE.

it continues to be the fourth most life-threatening infectious syndrome (11, 12). Infection-related endothelial damage leads to cell death and surface deterioration (1). Further damage and infarction may occur if endocarditis progresses into myocarditis or if vegetation causes coronary artery embolization. This damage and infarction may be seen on cardiac MRI. Myocardial damage can be demonstrated noninvasively by detecting gadolinium contrast enhancement in the late phase (13). These areas of late-phase contrast enhancement have been shown to be consistent with irreversible myocardial damage and fibrosis (14). However, delayed contrast enhancement of the endothelial lining in IE has not been previously studied except in a case report (10).

While most of the known complications of IE are observed far from the

source of infection due to distribution by blood flow, some complications have been shown to occur in close proximity to the source. For instance, regurgitant jet flows and intracardiac shunt may lead to development of lesions. Infections in the right ventricle that form due to jet flows in VSDs with left-to-right shunt can be attributed to the relative blood stasis in these areas. Endocarditis of the tricuspid valve and the right ventricular wall has been reported in such small high-flow VSDs. However, direct endothelial damage can occur in any high-pressure flow area (14, 15). In the present study, dissemination of the endocarditis was depicted by MRI. In the presence of VSD, delayed contrast enhancement was detected on the lateral wall of the right ventricle due to high-pressure jet causing direct endothelial damage and on the right surface of the proximal in-

terventricular septum adjacent to the VSD secondary to the stasis (Fig. 5).

Endocardial jet lesions can also be found in patients with aortic regurgitation. Regurgitant jets may lead to infection, aneurysm, and perforation of the anterior mitral leaflet and chordae tendineae (15). In our study, contrast enhancement secondary to antegrade dissemination was observed on all segments of the aorta and superior mesenteric artery in a 48-year-old man with aortic valve vegetation. Retrograde dissemination of the infection to the mitral valve due to aortic insufficiency was also present in the same patient (Fig. 3). These two exemplary cases and six other cases, in which antegrade dissemination of the infection to the aorta and pulmonary artery was detected, indicate that cardiac MRI can depict the retrograde or antegrade dissemination of the infection regardless of the presence of vegetation or embolization.

Surgical intervention is generally required if infection reaches the tissues surrounding the valves. Paravalvular extension of infection may result in endothelial erosion, paravalvular abscess, mycotic aneurysm, and intracardiac fistula (16). In order to eradicate infection and normalize hemodynamics in such cases, procedures like abscess drainage, excision of necrotic tissue, and fistula tract closure are performed along with valve replacement surgery (17, 18). The more severe the paravalvular involvement, the more difficult it is for the surgeon to ensure the anatomic integrity and functionality of the heart following excision of infected tissues (19–21).

On both TTE and TEE, paravalvular extension may be detected when a complication like abscess or fistula occurs (22–24). Fortunately, in the current study it was possible to detect the paravalvular extension of the infection by MRI, depicting delayed contrast enhancement on the paravalvular tissues in six patients before complications arose (Figs. 2 and 4).

A timely diagnosis of IE is required in order to implement appropriate treatment and reduce the risk of morbidity and mortality. Clinical signs of IE are many and varied. As the clinical presentation varies depending on

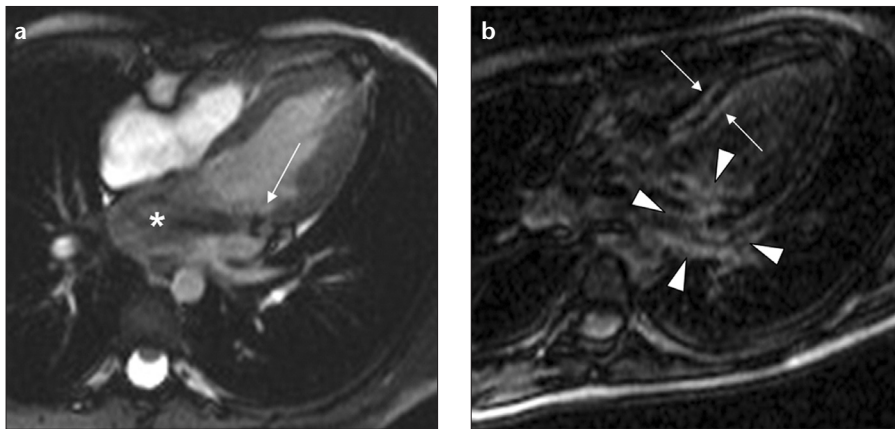


Figure 4. a, b. Cine and delayed enhanced cardiac images show direct and flow-related extension to the adjacent tissue and endocardium in a six-year-old girl. Cine image (a) shows two vegetations on the mitral valve (arrow) and signal changes due to severe mitral valve insufficiency (asterisk). Postcontrast image (b) shows delayed contrast enhancement secondary to direct extension of the infection in the adjacent paravalvular tissue (arrowheads) and right and left ventricular endocardial surface of the interventricular septum secondary to flow-related extension of the infection (arrows).

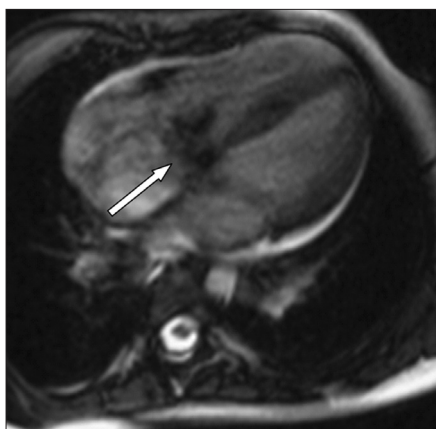


Figure 5. Left-to-right jet flow through the ventricular septal defect (arrow) is observed on cine images in a four-year-old girl.

factors like disease duration, the type of microbial factor, the affected valve, and patient age, diagnosing IE can be a challenge and outcomes are difficult to predict (25). In patients with clinical suspicion of endocarditis, vegetation is successfully detected with TTE in 50% of cases (16, 26). TEE can be inconclusive particularly in the early stages of the disease, when the size of the vegetation is too small for detection (27). Likewise, MRI may also miss the vegetations as seen in our study. However, regardless of the absence of vegetations on MRI, the determination of delayed contrast enhancement of the endothelial lining can reveal the diagnosis of endocarditis.

Several studies have demonstrated that multiple echocardiographic stud-

ies may be useful when determining the prognosis for IE patients. Whether multiple procedures are excessive is open to debate. Vieira et al. (28) evaluated 262 patients with endocarditis suspicion referred for echocardiography, over the course of three years. The average number of TTE procedures in their study was 2.4; in six cases, TTE was performed six times. Also, TEE was performed an average of 1.7 times, four times in four cases and five times in one case. Complications like oral benzocaine spray-related methemoglobinemia, Mallory-Weiss tear after intraoperative TEE, thoracic esophageal rupture and fatal arrhythmia have been reported in several cases (29). In very small infants, potential airway compression risk, vascular pressure and damage to the oral cavity, teeth, esophagus, and gastric mucosa have been reported (30, 31). In addition to these complications, intolerance of TEE is a frequently observed limitation of this procedure, particularly in the pediatric population. Though the number of patients included in this study was limited, our findings showed that in cases with high clinical suspicion of IE, MRI could be an alternative imaging tool to repeated TTE or TEE examinations in order to reveal the diagnosis and to avoid the potential complications.

Differential diagnosis of vegetation includes myxomas, thrombi, lipomas, and papillary fibroelastomas (32). Myxomas usually demonstrate characteristic mobility on cine gradient-echo

images. They show early moderate heterogeneous enhancement and delayed high heterogeneous enhancement after contrast administration. Contrast-enhanced cardiac MRI reveals thrombi as low-signal-intensity, because they are avascular. Lipomas demonstrate signal suppression on fat-saturated sequences. Papillary fibroelastomas appear as hypointense mobile masses on cine gradient-echo images which show high signal intensity after contrast administration (33, 34).

The limitations of our study are the absence of histopathological confirmation of inflammation of the endothelial lining, lack of cardiac MRI follow-up, and the relatively small number of patients. Also, metallic artifacts due to prosthetic valves may limit the diagnostic value of MRI examination.

In conclusion, cardiac MRI can be a valuable examination method to detect vegetations in patients with suspected IE. Furthermore, MRI can give valuable diagnostic and prognostic information about the disease by depicting features such as the antegrade and retrograde dissemination, paravalvular tissue extension, and subendocardial and vascular endothelial involvement on delayed contrast-enhanced images. We suggest that cardiac MRI should have a role in the diagnostic algorithm for IE.

Conflict of interest disclosure

The authors declared no conflicts of interest.

References

1. Bashore TM, Cabell C, Fowler V Jr. Update on infective endocarditis. *Curr Probl Cardiol* 2006; 31:274–352. [CrossRef]
2. Karchmer A. Infective endocarditis. In: Zipes DP, Libby P, Bonow RO, et al, eds. *Heart Disease*. Philadelphia: Elsevier Saunders, 2005; 1633–1656.
3. Rodbard S. Blood velocity and endocarditis. *Circulation* 1963; 27:18–28. [CrossRef]
4. Netzer RO, Zollinger E, Seiler C, Cerny A. Infective endocarditis: clinical spectrum, presentation, and outcome. An analysis of 212 cases 1980–1995. *Heart* 2000; 84:25–30. [CrossRef]
5. Todd AJ, Leslie SJ, Macdougall M, Denver MA. Clinical features remain important for the diagnosis of infective endocarditis in the modern era. *QJM* 2006; 99:23–31. [CrossRef]
6. Durack DT, Lukes AS, Bright DK. New criteria for diagnosis of infective endocarditis: utilization of specific echocardiographic findings. Duke Endocarditis Service. *Am J Med* 1994; 96:200–209. [CrossRef]

7. Caduff JH, Hernandez RJ, Ludomirsky A. MR visualization of aortic valve vegetations. *J Comput Assist Tomogr* 1996; 20:613–615. [\[CrossRef\]](#)
8. Pollak Y, Comeau CR, Wolff SD. Staphylococcus aureus endocarditis of the aortic valve diagnosed on MR imaging. *AJR Am J Roentgenol* 2002; 179:1647. [\[CrossRef\]](#)
9. Sievers B, Brandts B, Franken U, Trappe HJ. Cardiovascular magnetic resonance imaging demonstrates mitral valve endocarditis. *Am J Med* 2003; 115:681–682. [\[CrossRef\]](#)
10. Dursun M, Yilmaz S, Ali Sayin O, et al. A rare cause of delayed contrast enhancement on cardiac magnetic resonance imaging: infective endocarditis. *J Comput Assist Tomogr* 2005; 29:709–711. [\[CrossRef\]](#)
11. Berlin JA, Abrutyn E, Strom BL, et al. Incidence of infective endocarditis in the Delaware Valley, 1988–1990. *Am J Cardiol* 1995; 76:933–936. [\[CrossRef\]](#)
12. Bayer AS, Bolger AF, Taubert KA, et al. Diagnosis and management of infective endocarditis and its complications. *Circulation* 1998; 98:2936–2948. [\[CrossRef\]](#)
13. Rehwald WG, Fieno DS, Chen EL, Kim RJ, Judd RM. Myocardial magnetic resonance imaging contrast agent concentrations after reversible and irreversible ischemic injury. *Circulation* 2002; 105:224–229. [\[CrossRef\]](#)
14. Kim RJ, Wu E, Rafael A, et al. The use of contrast-enhanced magnetic resonance imaging to identify reversible myocardial dysfunction. *N Engl J Med* 2000; 343:1445–1453. [\[CrossRef\]](#)
15. Gregory SA, Yepes CB, Byrne JG, D'Ambra MN, Chen MH. Atrial endocarditis—the importance of the regurgitant jet lesions. *Echocardiography* 2005; 22:426–430. [\[CrossRef\]](#)
16. Evangelista A, Gonzalez-Alujas MT. Echocardiography in infective endocarditis. *Heart* 2004; 90:614–617. [\[CrossRef\]](#)
17. Baddour LM, Wilson WR, Bayer AS, et al. Infective endocarditis: diagnosis, antimicrobial therapy, and management of complications: statement for healthcare professionals from the Committee on Rheumatic Fever, Endocarditis, and Kawasaki Disease, Council on Cardiovascular Disease in the Young, and the Councils on Clinical Cardiology, Stroke, and Cardiovascular Surgery and Anesthesia, American Heart Association: endorsed by the Infectious Diseases Society of America. *Circulation* 2005; 111:394–434. [\[CrossRef\]](#)
18. Mullany CJ, Chua YL, Schaff HV, et al. Early and late survival after surgical treatment of culture-positive active endocarditis. *Mayo Clin Proc* 1995; 70:517–525. [\[CrossRef\]](#)
19. Pomerantzeff PM, de Almeida Brandao CM, Albuquerque JM, et al. Risk factor analysis of hospital mortality in patients with endocarditis with ring abscess. *J Card Surg* 2005; 20:329–331. [\[CrossRef\]](#)
20. Glazier JJ, Verwilghen J, Donaldson RM, Ross DN. Treatment of complicated prosthetic aortic valve endocarditis with annular abscess formation by homograft aortic root replacement. *J Am Coll Cardiol* 1991; 17:1177–1182. [\[CrossRef\]](#)
21. Ross D. Allograft root replacement for prosthetic endocarditis. *J Card Surg* 1990; 5:68–72. [\[CrossRef\]](#)
22. Jenkins NP, Habib G, Prendergast BD. Aorto-cavitary fistulae in infective endocarditis: Understanding a rare complication through collaboration. *Eur Heart J* 2005; 26:213–214. [\[CrossRef\]](#)
23. Anguera I, Miro JM, Vilacosta I, et al. Aorto-cavitary fistulous tract formation in infective endocarditis: clinical and echocardiographic features of 76 cases and risk factors for mortality. *Eur Heart J* 2005; 26:288–297. [\[CrossRef\]](#)
24. Choussat R, Thomas D, Isnard R, et al. Perivalvular abscesses associated with endocarditis; clinical features and prognostic factors of overall survival in a series of 233 cases. *Perivalvular Abscesses French Multicentre Study. Eur Heart J* 1999; 20:232–241. [\[CrossRef\]](#)
25. Tansel T, Onursal E, Eker R, Ertugrul T, Dayioglu E. Results of surgical treatment for infective endocarditis in children. *Cardiol Young* 2005; 15:621–626. [\[CrossRef\]](#)
26. Muggé A, Daniel WG, Frank G, Lichtlen PR. Echocardiography in infective endocarditis: reassessment of prognostic implications of vegetation size determined by the transthoracic and the transesophageal approach. *J Am Coll Cardiol* 1989; 14:631–638. [\[CrossRef\]](#)
27. Law A, Honos G, Huynh T. Negative predictive value of multiplane transesophageal echocardiography in the diagnosis of infective endocarditis. *Eur J Echocardiogr* 2004; 5:416–421. [\[CrossRef\]](#)
28. Vieira ML, Grinberg M, Pomerantzeff PM, Andrade JL, Mansur AJ. Repeated echocardiographic examinations of patients with suspected infective endocarditis. *Heart* 2004; 90:1020–1024. [\[CrossRef\]](#)
29. Coleman JM, Haider B, Cuyjet AB, Zakir RM, Riauba L, Saric M. Fatal ascending aorta-to-right ventricle fistula formation after Staphylococcus aureus endocarditis of bicuspid aortic valve. *Heart Lung* 2005; 34:429–432. [\[CrossRef\]](#)
30. Sheil ML, Baines DB. Intraoperative transoesophageal echocardiography for paediatric cardiac surgery—an audit of 200 cases. *Anaesth Intensive Care* 1999; 27:591–595.
31. Stevenson JG, Sorenson GK. Proper probe size for pediatric transesophageal echocardiography. *Am J Cardiol* 1993; 72:491–492. [\[CrossRef\]](#)
32. Eslami-Varzaneh F, Brun EA, Sears-Rogan P. An unusual case of multiple papillary fibroelastoma, review of literature. *Cardiovasc Pathol* 2003; 12:170–173. [\[CrossRef\]](#)
33. O'Donnell DH, Abbara S, Chaithiraphan V, et al. Cardiac tumors: optimal cardiac MR sequences and spectrum of imaging appearances. *AJR Am J Roentgenol* 2009; 193:377–387. [\[CrossRef\]](#)
34. Sparrow PJ, Kurian JB, Jones TR, Sivanathan MU. MR imaging of cardiac tumors. *Radiographics* 2005; 25:1255–1276. [\[CrossRef\]](#)